Tellus
SERIES A
DYNAMIC
METEOROLOGY
AND OCEANOGRAPHY
PUBLISHED BY THE INTERNATIONAL METEOROLOGICAL INSTITUTE IN STOCKHOLM

*Tellus (2010), 62A, 569–578*



TELLUS

# Interannual to multidecadal variability and predictability of North Atlantic circulation in a coupled earth system model with parametrized hydraulics

*By* M. KÖLLER[1]*, R. H. KÄSE[1] and P. HERRMANN[2], [1]*Institute of Oceanography, University of Hamburg, D-20146 Hamburg, Germany;* [2]*Max Planck Institute for Meteorology, Hamburg, Germany*

(Manuscript received 17 July 2009; in final form 23 March 2010)

ABSTRACT

Several 1000 yr runs of the University of Victoria Earth System Climate Model (UVic ESCM) with a hydraulically controlled overflow in the Denmark Strait are used to analyse the effects of NAO-like variations of the wind stress localized in the subpolar North Atlantic. The focus is laid on improving the representation of the Atlantic meridional overturning circulation (AMOC), the sea surface temperatures in the Nordic Seas and the sea ice coverage without increasing the resolution of the global model. We show that by implementing hydraulic control in the Denmark Strait Overflow the AMOC can be enhanced at depths between 1000 and 3000 m by up to 7 Sverdrup (Sv) towards more realistic values. The stability of the Deep Western Boundary Current is considerably enhanced. The expansion of sea ice into the Nordic Seas in the standard run is pushed back from about 65°N to 75°N when hydraulic parametrization is switched on. In this case sea ice variations at 75°N and Northern Europe air temperatures exhibit a lag of 9 yr to variations in the wind stress curl.

## 1. Introduction

The Denmark Strait can be seen as a key region for present-day climate, as about one half of the water masses that later become North Atlantic Deep Water is related to exchange processes via this passage (e.g. Cooper, 1955; Ross, 1984; Quadfasel and Käse, 2007). The outflow of waters over this sill is limited by hydraulic control (e.g. Whitehead, 1998; Käse and Oschlies, 2000; Girton et al., 2001). Several different model studies showed that an overflow parametrization based on hydraulic constraints leads to a more realistic representation of the Denmark Strait Overflow (Kösters et al., 2005), a stronger AMOC and temperatures and salinities in the Nordic Seas that remain closer to observed values (Born et al., 2009). Moreover, the sea ice edge is located much further northwards, again in a better agreement with observations (Kösters et al., 2005).

Saunders et al. (2008) noted the persisting problem that ocean models picture a much too shallow AMOC. Spence et al. (2008) demonstrated that improvements in the barotropic volume transports, the meridional heat transport and the poleward penetration of the North Atlantic Current can be obtained by increasing the spatial resolution of the respective model. In this study we maintain the original coarse resolution of 3.6° (zonal) x 1.8° (meridional) to save on computing time, as we accomplish several 1000 yr runs in a global model.

A major factor defining the European climate variability is the North Atlantic Oscillation (NAO, e.g. Hurrell, 1996; Greatbatch, 2000). Recent variability of the NAO since the 1950s is mimicked in several climate variables like in the number of frost days (Meehl et al., 2004), the occurrence of extreme events (e.g. Cavazos, 2000) and fish catch (Reid et al., 2001). Hilmer and Jung (2000) found a high correlation between the NAO and Arctic sea ice export through Fram Strait after 1977. Köberle and Gerdes (2003) showed a significant contribution of the wind stress forcing in their ocean–sea ice model to the decadal variability in the Arctic ice volume.

Some focus will be laid on the Labrador Sea region. Latif et al. (2006) discovered a lagged correlation of the Labrador Sea convection depth and the North Atlantic/South Atlantic sea surface temperature dipole of about 11 yr, with the NAO unlagged to convection. It is not clear whether further prognostic capabilities are hidden in other NAO-conditioned correlations. The difficulties lie in the short time series available that lead to large significance margins. Therefore we carry out multicentennial and millenium scale runs by employing artificial wind stress forcing variability with zero mean on the equilibrium

*Corresponding author.
e-mail: matthias.koeller@zmaw.de
DOI: 10.1111/j.1600-0870.2010.00450.x

state to prove and expand the findings of Kösters et al. (2005) concerning implementation of hydraulic control and to see if any lagged correlations can be found that might establish climate predictabilities.

The paper is structured as follows. In Section 2, we describe the model setups, in Sections 3.1–3.3 we discuss the improvements made by the hydraulic parametrization to the mean ocean state. We continue to apply different wind stress forcing scenarios in the subpolar North Atlantic, that differ by their time spectrum only. This is done in Section 4. The emerging lagged correlations between subtropic/subpolar diagnostic quantities and the Nordic Seas ice cover or Northern Europe air temperature are established. In the discussion section we try to relate our findings to recent observations and numerical experiments.

## 2. Model description

Our investigations are based on version 2.8 of the University of Victoria Earth System Climate Model (UVic ESCM), which is a model of intermediate complexity. Its components are a three-dimensional ocean general circulation model coupled to a dynamic–thermodynamic sea ice model, a land- and vegetation model and an energy-moisture balance atmosphere model with dynamical feedbacks. Its first release is described in detail in Weaver et al. (2001). The ocean component is version 2.2 of the Geophysical Fluid Dynamics Laboratory Modular Ocean Model (GFDL-MOM, Pacanowski, 1995). It consists of 19 unequally distributed vertical levels, reaching from a 50-m-thick near surface layer to a 518-m-thick bottom layer at greatest depths. The global coupled model has a resolution of 3.6° (zonal) by 1.8° (meridional). Atmospheric heat and fresh water transport are achieved by advection through monthly climatological near-surface winds, and Fickian diffusion. Precipitation occurs when the relative humidity is greater than 85%. Even though the wind field is fixed, there is a dynamical feedback between atmosphere and ocean on diffusive timescales.

The AMOC in the UVic ESCM has been shown to be sensitive to diverse parametrizations. For example, Wiebe and Weaver (1999) showed a sensitivity in the ocean component of the UVic ESCM to the Gent and Mc Williams parametrization for mixing with mesoscale eddies and Saenko et al. (2003) revealed a sensitivity of the AMOC in the UVic ESCM to meridional moisture transport and freshening in the Southern Ocean.

Due to the relatively coarse grid, several shortcomings occured in previous simulations. If the model is driven to equilibrium, the ocean's thermohaline structure without restoring towards climatology is deviating considerably from the observed mean state. To overcome this partly, we apply a parametrization of the dense water exchange through the Denmark Strait, which is a major site for the export of Nordic Seas' water into the deep subpolar North Atlantic. About one half of the water masses that later become North Atlantic Deep Water is related to exchange processes via this passage. Therefore, the first experiments focus on the improvements in water mass distribution obtained from this parametrization. The run labelled CONTR is a standard control run with parameters set as in the reference run of the UVic ESCM (Weaver et al., 2001). The only change in run HYD compared to CONTR is the parametrized dense overflow in the Denmark Strait.

Details of the hydraulic parametrization are described in Kösters (2004) and Kösters et al. (2005). The main procedure is to replace the advective and diffusive fluxes according to the diagnosed hydraulic transport in the bottom cell at the sill. As the basic equation for the maximum hydraulic transport we use the integral

$$Q = \frac{g}{f\rho_0}\int_h^0 (\rho_N(z) - \rho_S(z))\, z\, \mathrm{d}z, \tag{1}$$

with $g$ being the gravitational acceleration, $f$ the Coriolis parameter, $\rho_0$ the mean density, $\rho_N$ and $\rho_S$ the laterally averaged but depth dependent potential densities north and south of the sill and the integral being evaluated from sill depth $z = h$ to surface $z = 0$. For constant densities $\rho_N$ and $\rho_S$ the integral reduces to equation 12 of Whitehead (1998). This parametrization is also used in the runs HYDP and HYDW, where an additional wind stress forcing is applied over the subpolar North Atlantic. This additional forcing has the spectral form of pink and white noise, respectively. In NHYDP and NYHDW exactly the same forcings are used but hydraulic control is switched off again. Table 1 gives an overview of the six different runs.

Our motivation to use different wind stress forcings was to detect the influences of the NAO on variations in the sea ice

*Table 1.* Characteristics of the six different model runs.

| Time range (yr) | Hydraulic control implemented | Wind spectral form | Acronym |
|---|---|---|---|
| 3601–5500 | No | Climatological | CONTR |
| 3601–5500 | Yes | Climatological | HYD |
| 0–5500 | Yes | Climatological + pink noise | HYDP |
| 3601–5500 | Yes | Climatological + white noise | HYDW |
| 3601–5500 | No | Climatological + pink noise | NHYDP |
| 3601–5500 | No | Climatological + white noise | NHYDW |

coverage, barotropic streamfunction, salinities, etc. The pink noise (or $1/f$) forcing seemed to be an appropriate alternative to the white noise forcing as this kind of spectral form consistently appears in nature (e.g. Hooge, 1976; Yano et al., 2000; Fraedrich and Blender, 2003). A pink noise low frequency spectrum can be the result of random perturbation on a dominant peak frequency (Kaulakys and Meškauskas, 1999), which in our case would be corresponding to the seasonal cycle. Thus, instead of reconfiguring the basic climatological forcing, we superimpose pink noise wind stress curl variations on the seasonal climatology. Regarding observations, a test for autoregression of the station based monthly NAO is not successful. However, the recent variability documented in the winter NAO since 1970 indicates some longer term memory. It is therefore interesting to note that the spectrum of a 2 yr running mean winter NAO is statistically not different from pink noise.

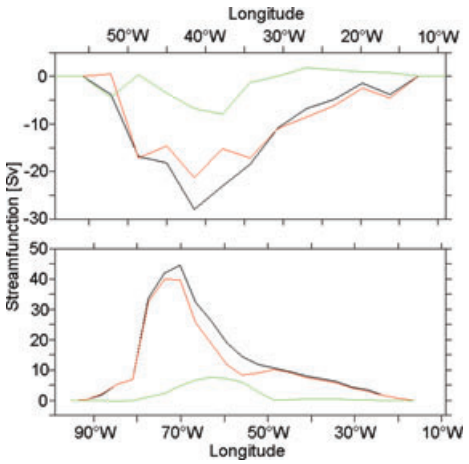


*Fig. 2.* Section through subpolar (at 55°N, upper panel) and subtropical gyre (at 25°N, lower panel). Black: HYDP, red: NHYDP, green: HYDP-NHYDP.

## 3. Improvements through implementation of hydraulic control in the Denmark Strait

### *3.1. Barotropic Gyres*

The barotropic streamfunction in the case of no hydraulic parametrization is displayed in Fig. 1a. The North Atlantic maximum subtropical transport is 40 Sv, the subpolar gyre exhibits hardly 20 Sv. The barotropic circulation around Iceland is much less than 5 Sv. In the southern hemisphere the subtropical gyre is 25–30 Sv while the circumpolar current reaches close to 100 Sv. The improvement by introducing the hydraulic parametrization can immediately be seen in the difference plot HYDP-NHYDP (Fig. 1b). A section through both the subtropical and subpolar gyres in Fig. 2 displays the absolute values. The subtropical gyre (lower plot) is enhanced by 8 Sv and widened to the east. The subpolar gyre in the Irminger Sea has increased by 8–10 Sv. Also, the Nordic Seas have a distinct Greenland Sea gyre now and the circulation around Iceland has increased to more than 6 Sv. The changes in the circumpolar current, which are of the order of the North Atlantic Current increase, have the opposite sign, reducing the strength of the flow through Drake Passage.

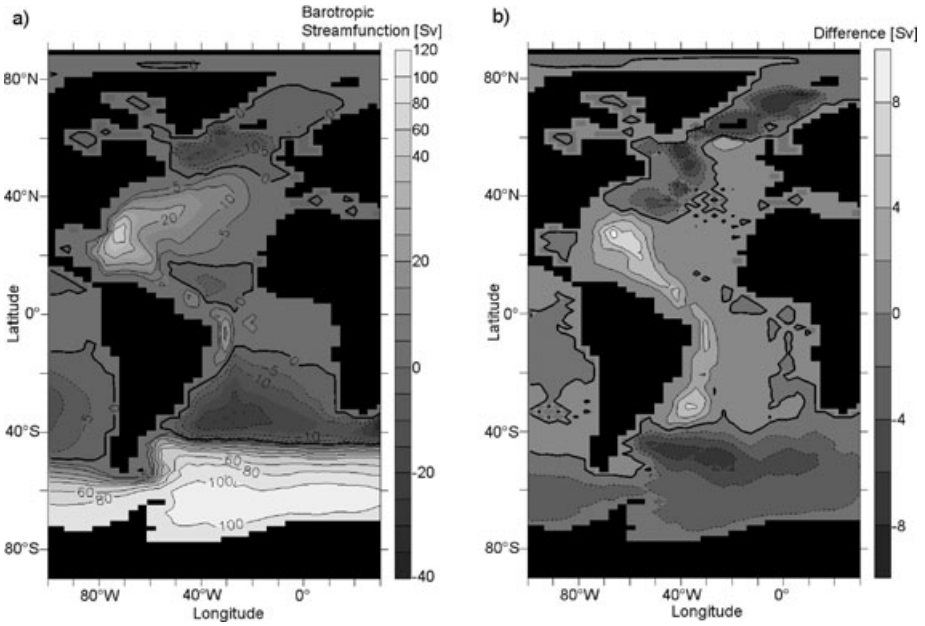


*Fig. 1.* Time-averaged Atlantic barotropic streamfunction for run NHYDP (a). The difference plot between HYDP and NHYDP shows the changes that occur through hydraulic control parametrization in the Denmark Strait (b).

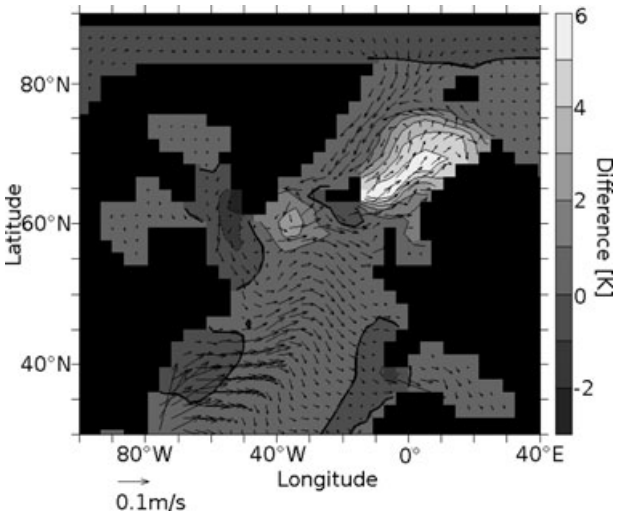


*Fig. 3.* Difference in sea surface temperature between HYDP and NHYDP. The implementation of hydraulic control results in a warming in the Nordic Seas. Additionally, the mean surface velocity vectors of the HYDP run are plotted.

### 3.2. *Surface fields*

The increased gyre strength obtained by implementing hydraulic constraints into the parametrization of the Denmark Strait Overflow in addition yields a surface warming in the Nordic Seas (Fig. 3). This leads to a closer agreement with the Levitus climatology (Levitus, 1982) which can be seen in Fig. 4a. The equivalent salt increase is shown in Fig. 4b. The 34-PSU-isohaline is shifted into the western part of the Nordic Seas and towards Spitsbergen in the north. However, there is no pronounced West Spitsbergen Current in the mean and most of the warm and salty waters are entering the Arctic through the Barents Sea opening, probably because of the unresolved topography. As a consequence, the ice edge (not shown) is pushed back from about 65°N in NHYDP to about 75°N in HYDP which confirms the findings of Kösters et al. (2005) and is in a better accordance with observations. This was also confirmed by Born et al. (2009) who used the Kösters et al. (2005) parametrization in the coupled climate model CLIMBER-3$\alpha$ (Montoya et al., 2005).

### 3.3. *Overturning*

In the introduction it was brought up that in general the AMOC is displayed too shallow in ocean models (Saunders et al., 2008). The contours in Fig. 5a show the vertical structure of the mean NHYDP overturning, while in Fig. 5b the overturning for the HYDP run is shown. It is obvious that the hydraulic control parametrization strengthens the transport at depths between 1000 and 3000 m by up to 7 Sv. The figures also show that the downstream representation of water masses is improved, which

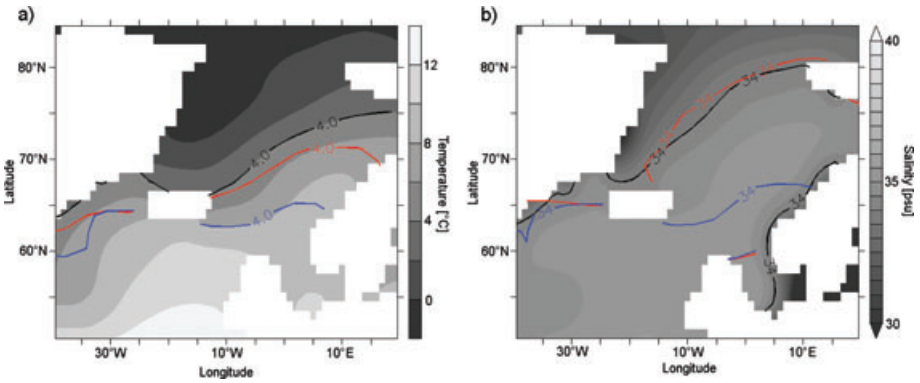


*Fig. 4.* Comparison of the 4°C isotherm (left) and the 34-PSU-isohaline (right) in the runs HYDP (red line), NHYDP (blue line) and the Levitus climatology (grey background, black line).

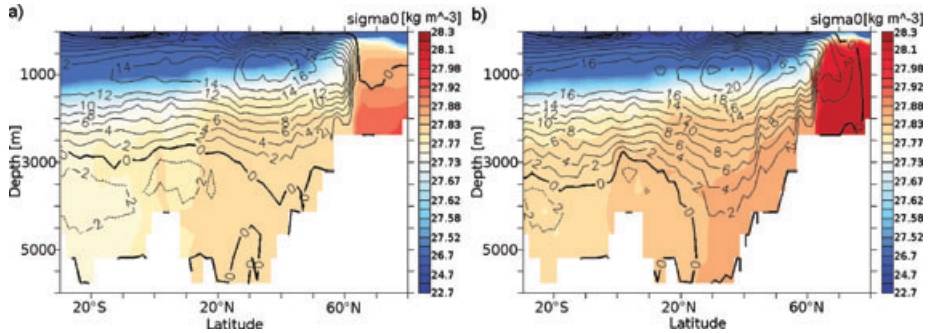


*Fig. 5.* AMOC streamfunction (Sv, black) contoured over Density Anomaly in NHYDP (a) and HYDP (b). Through implementation of hydraulic control in the Denmark Strait higher, denser and thus more realistic transport rates are achieved.

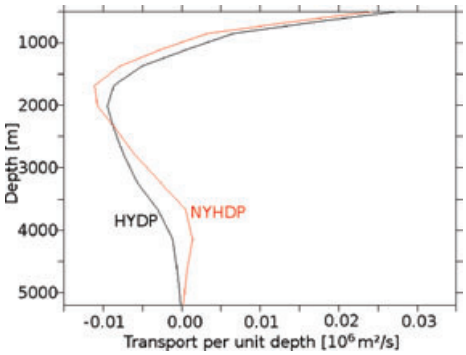


*Fig. 6*. Comparison between cross-sections of transport per unit depth at 25°N in runs HYDP and NHYDP. Implementation of hydraulic control leads to a broader and deeper core.

is visible in the extent of the tongue of deep water with $\sigma_0 \geq 27.8$ kg m$^{-3}$ south of Denmark Strait.

A comparison between the cross-section of the derivation of the overturning (Fig. 6) and observations (e.g. shown in Roemmich and Wunsch, 1985; Döscher et al., 1994) shows that the lack of a second core at about 4000 m depth persists. This may be ascribed to the coarse resolution of only 19 vertical levels. On the other hand, in the runs with hydraulic control the first core is broadened and shifted to greater depths, in a better agreement with observations.

In Fig. 7 the velocity vectors at 3658 m depth (15th layer) of the NHYDP run are subtracted from the corresponding vectors

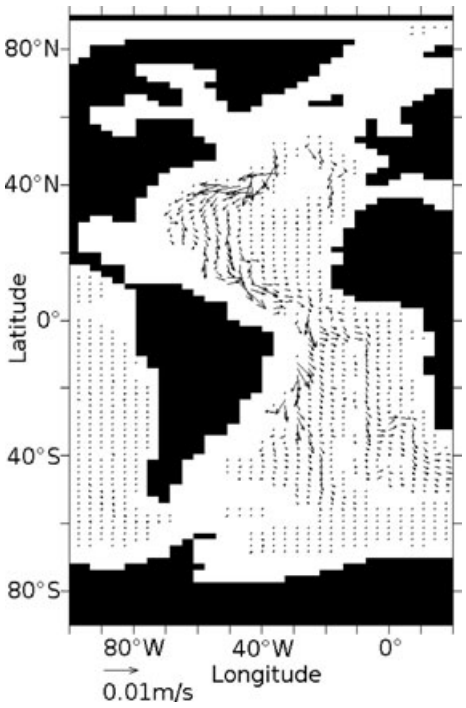


*Fig. 7*. Velocity vectors at 3658 m depth from NHYDP run subtracted from equivalent velocities in HYDP. In the run with hydraulic control a stronger Western Boundary Current emerges.

of the HYDP run. The result shows a strengthening of the Deep Western Boundary Current when hydraulic control is switched on. The stabilizing effect of the hydraulic control parametrization is seen in Hovmoeller diagrams of the southward transport of water with $\sigma_0 \geq 27.8$ kg m$^{-3}$ west of 30°W (Fig. 8). In the non-hydraulic case, variations are about 50% larger, and the Deep Western Boundary Current temporarily disappears, indicating a thermohaline off-state (white patches represent non-existing NADW). Southward propagation is accelerated from 0.41 cm s$^{-1}$ in NHYDP to 1.45 cm s$^{-1}$ in HYDP, as the parametrization acts as a source of momentum.

The strengthening of the overturning circulation also translates in more realistic heat transports (e.g. shown in Talley et al., 2003). In the runs without anomalous wind stress forcing the heat transport across 45°N gets enhanced from 0.47 PW in CONTR to 0.68 PW in HYD, the runs with white noise forcing show an enhancement from 0.52 PW in NHYDW to 0.68 PW in HYDW and in the pink noise forced runs it rises from 0.51 PW in NHYDP to 0.68 PW in HYDP.

## 4. Influence of varying wind stress curl in the North Atlantic

As described in Section 2 and shown in Table 1, two different wind stress forcings were used, having the spectral form of pink noise in HYDP and NYHDP on the one hand and white noise in HYDW and NHYDW on the other hand. As pointed out in the previous chapters, the runs with hydraulic control parametrization show a better agreement with observations. Hence we concentrate on them when looking at the influence of varying wind stress curl in the North Atlantic.

A horizontally Gaussian shaped anomaly in wind stress curl is superimposed on the climatological forcing. The time dependence of the pink noise forcing anomaly can be seen in Fig. 9a. Figure 9b shows the time series for the white noise case. A higher positive forcing anomaly leads to a stronger cyclonic rotation in the wind field. As a curlplus ensemble we define all samples with higher forcing anomalies than one standard deviation. The curlminus ensemble is defined accordingly. The wind fields for these two ensembles are presented in Figs. 9c and 9d, respectively. The standard deviation of the forcing in the HYDP run is about twice as large as in the HYDW run. As a consequence, the influence of the varying wind stress curl becomes more apparent in the HYDP run, so that we only show figures from this run. However, the correlation coefficients and lags between different variables are also given for the HYDW run.

In the subpolar gyre region the strongest variations in the barotropic streamfunction emerged at 55°N. Therefore we calculated the gyre strength between 60°W and 30°W and analysed its correlations with other parameters. Unlagged correlations were found with the wind stress curl at 30°W and 55°N which is caused by the forcing ($R_{\mathrm{HYDP}} = -0.87$, Fig. 10a, $R_{\mathrm{HYDW}} = -0.76$), and with the surrounding average surface air

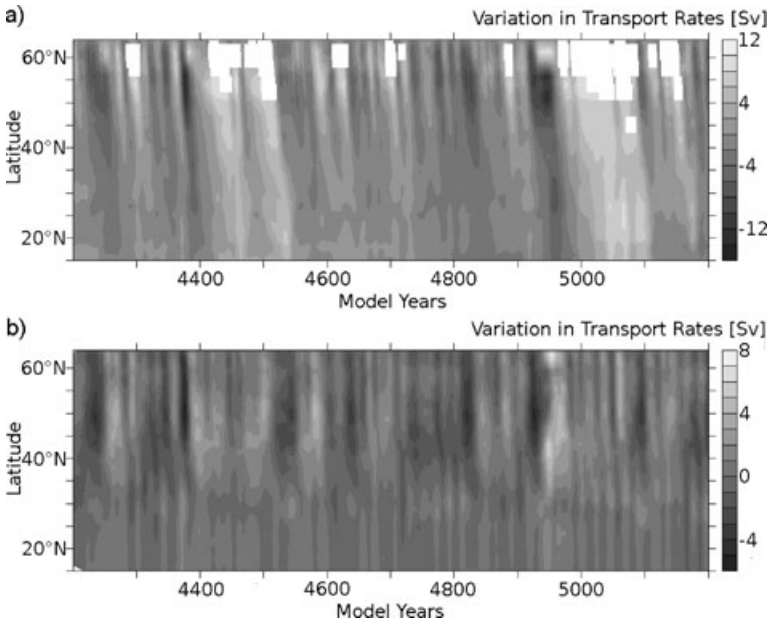


*Fig. 8.* Hovmoeller diagrams of the southward transport of dense water ($\sigma_0 \geq 27.8$ kg m$^{-3}$) in the NHYDP (a) and the HYDP (b) run. The southward propagation is accelerated and the variations are reduced to about 50% if hydraulic parametization is switched on. The white patches represent non-existing NADW.

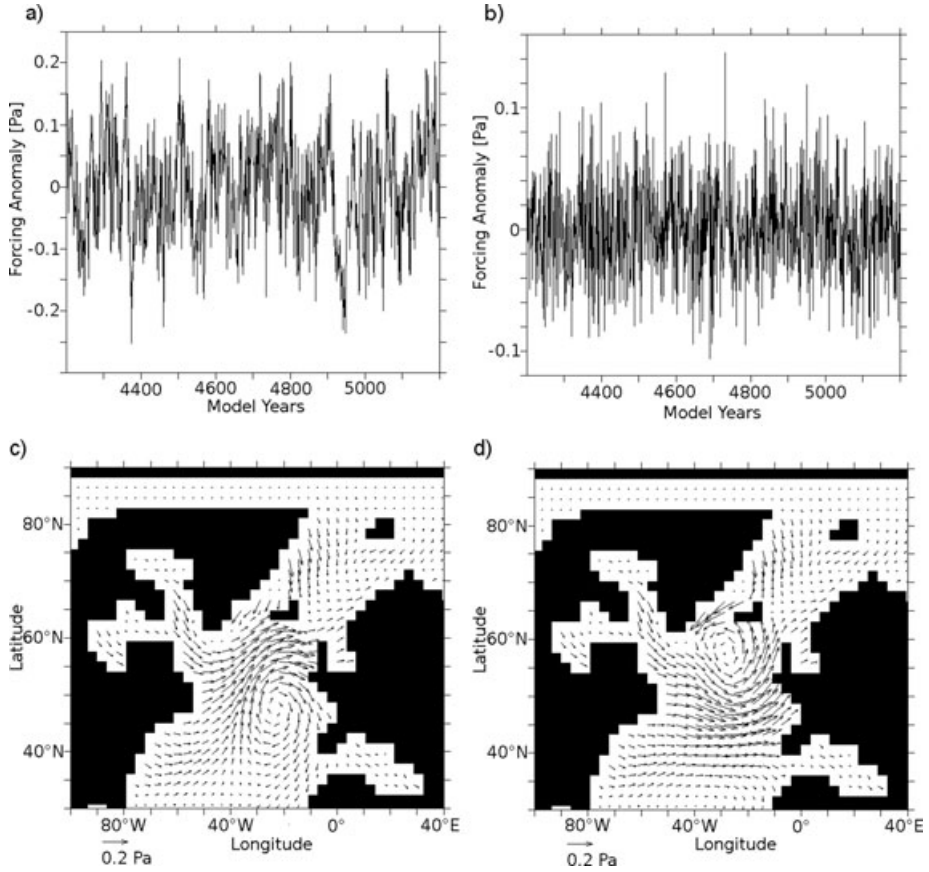


*Fig. 9.* Forcing of the pink noise (a) and white noise (b) experiments and the wind stress field in a curlminus (c) as well as in a curlplus ensemble (d).

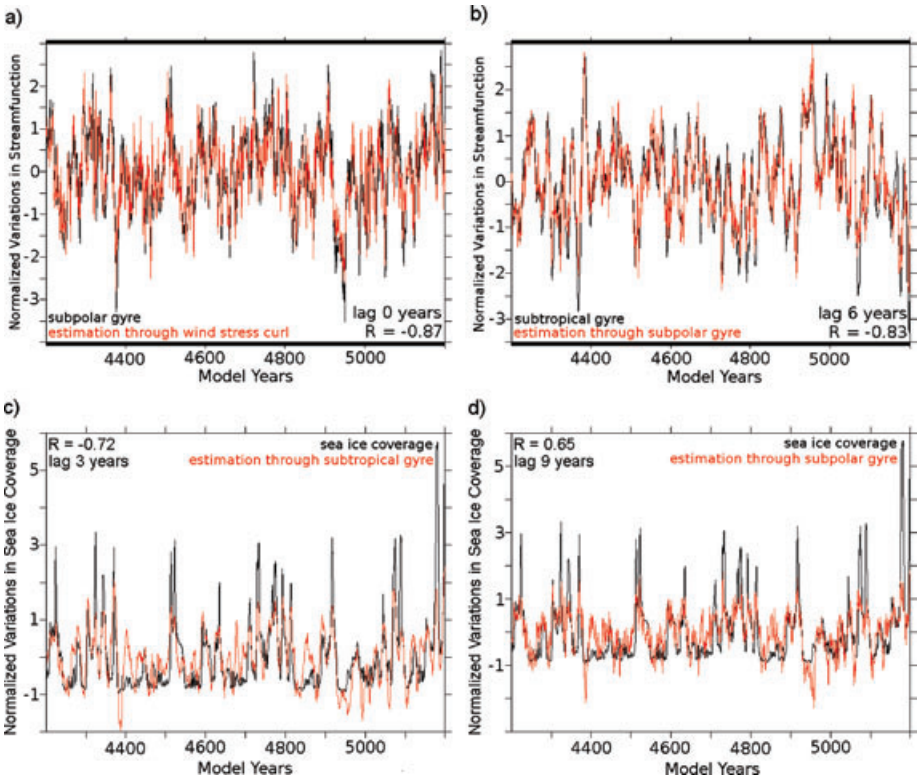


*Fig. 10.* Normalized variations (black) and their corresponding estimates from regression (red) for (a) subpolar gyre strength (black) and wind stress curl at 30°W, 55°N (red), (b) subtropical gyre strength (black) and subpolar gyre strength (red), (c) sea ice coverage at the sea ice edge at 75°N between 10°W and 10°E (black) and subtropical gyre strength (red), (d) the described sea ice coverage (black) and subpolar gyre strength (red). The denoted lags were removed and the estimation curves were inversed in case of negative correlation.

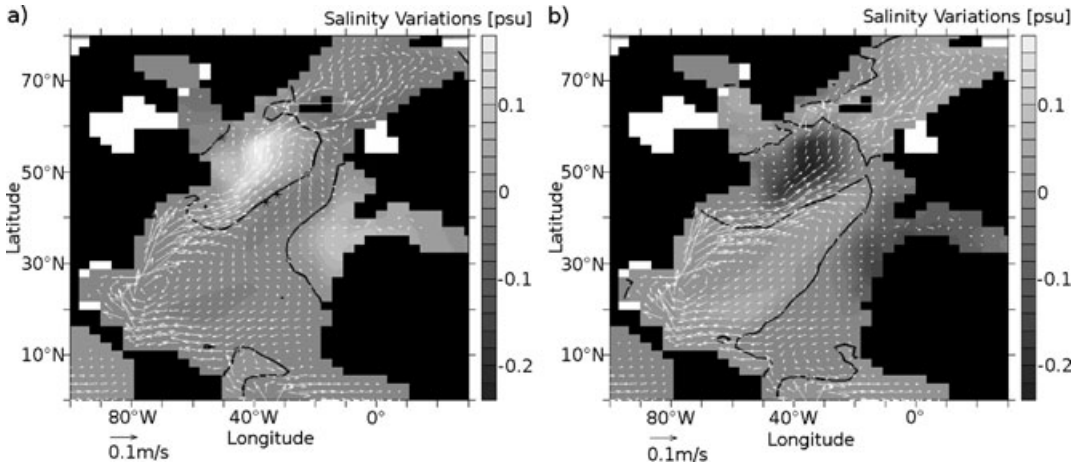


*Fig. 11.* Velocity vectors printed over salinity variations at 177 m depth in a curlminus (a) and a curlplus ensemble (b).

temperature in this region ($R_{\mathrm{HYDP}} = 0.81$, $R_{\mathrm{HYDW}} = 0.27$). Besides, the aforementioned variations lead variations in the subtropical gyre at 25°N by 6 yr. The correlation coefficient between the two is $R_{\mathrm{HYDP}} = -0.83$ (Fig. 10b) in the HYDP run and $R_{\mathrm{HYDW}} = -0.58$ in the HYDW run. A negative correlation results from increased vorticity in both gyres (more positive in subpolar and more negative in subtropical gyre or vice versa). The NAO-like forcing shifts the position of the subtropical and the subpolar gyre in an quasi-oscillating manner. This becomes apparent in Figs. 11a and b. Here the velocity vectors are plotted over the ocean salinity variations in the third layer at a depth of 177 m both for a curlplus and for a curlminus ensemble. When there is a strong positive wind stress curl phase, the border between the subpolar and the subtropical gyre is shifted southwards

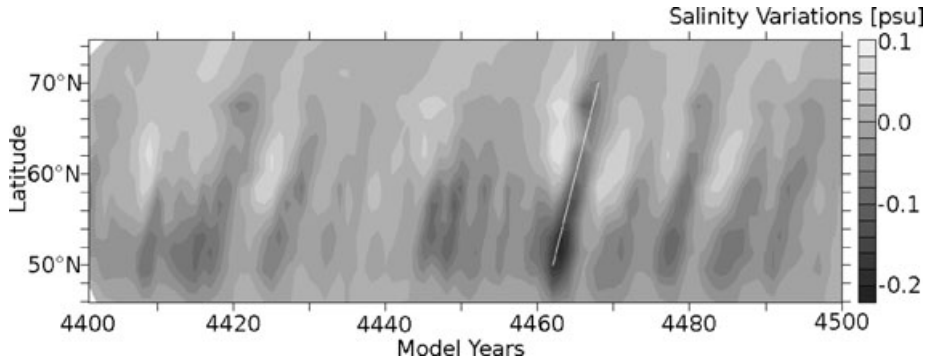


*Fig. 12.* Hovmoeller diagram of zonally averaged salinity anomalies for model years 4400–4500. It takes about 6 yr for the salinity variations to propagate from 50°N northwards to 70°N.

so that the North Atlantic Current gets enforced. Due to salinity conservation the time change in a given box is proportional to the flux out of its boundaries which is out of phase with the salinity itself. Since the peak in the variance conserving salinity spectrum (not shown) is at $7.4 \pm 3.6$ yr, we expect strongest advection 2 yr after the salinity maximum and 3 yr after that of the subpolar gyre streamfunction. This behaviour is consistent with the findings of Hátún et al. (2005), who could verify the observed increase of salinity in the Irminger Sea in case of a weak subpolar gyre, which again was discussed by Häkkinen and Rhines (2004). The advective process can be observed in Fig. 12, where the latitude- and time-dependent longitude-averaged salt variations are plotted. The marked line shows that the variations need about 6 yr to propagate from 50°N northwards to 70°N. The salt signal is used here, as in Hátún et al. (2005), because it mostly determines the density near freezing point temperature, and thus has the largest influence on the circulation in the Nordic Seas. Lagged correlations with the sea ice coverage at 75°N, averaged between 10°W and 10°E, emerge for both the variations in the subpolar gyre and the variations in the subtropical gyre. The lag between the subtropical gyre and the sea ice coverage is 3 yr in the HYDP run ($R_{\mathrm{HYDP}} = -0.72$, Fig. 10c) and 4 yr in the HYDW run ($R_{\mathrm{HYDW}} = -0.59$), whereas the subpolar gyre leads the sea ice coverage 9 yr in the HYDP run ($R_{\mathrm{HYDP}} = 0.65$, Fig. 10d) and 10 yr in the HYDW run ($R_{\mathrm{HYDW}} = 0.35$). The sea ice coverage moreover shows an unlagged correlation with Arctic temperatures ($R_{\mathrm{HYDP}} = -0.91$, $R_{\mathrm{HYDW}} = -0.87$).

## 5. Summary and discussion

Different model runs in the UVic ESCM confirmed and expanded the findings of Kösters et al. (2005) in millennium runs with different wind stress forcings that parameters like sea surface temperature, sea surface salinity, Denmark Strait Overflow transport, AMOC or sea ice coverage in the North Atlantic/Nordic Seas show a better agreement with observations when hydraulic control parametrization is switched on in the Denmark Strait. As a consequence, in future simulations it should be considered to expand such parametrizations for other hydraulically controlled passages, e.g. the Faroe Bank Channel. Spence et al. (2008) showed that a better spatial resolution also leads to more realistic model results. As we used a global model to perform our 1000 yr runs we maintained a coarse resolution. A combination of high resolution or a bottom boundary formulation as in Döscher and Beckmann (2000) and hydraulic control parametrization might result in even more realistic representations of oceanic fields.

Another aim of our studies was to investigate the effects of an NAO-like forcing. Several lagged correlations were found that yield the following schematics. The forcing affects the position of the subpolar and of the subtropical gyre. Variations in the barotropic streamfunction of the subtropical gyre lag variations in the barotropic streamfunction of the subpolar gyre by 6 yr. When the zero line of the wind stress curl is shifted more to the south, the North Atlantic Current becomes stronger and warmer and saltier waters enter the Nordic Seas. We have shown that a strong cyclonic subpolar gyre not only advects subpolar near surface water, but also entrains subtropical water that is being carried along the pathway of the North Atlantic Current. This process takes about 6 yr between 50°N and 70°N. The offset that occurs between the sea ice coverage at the sea ice edge at 75°N—being in phase with Arctic surface air temperatures—and the barotropic streamfunction in the subtropical gyre is 3 yr. Overall there is a 9 yr lag between the forcing or the gyre in the Labrador Sea region, respectively, and the sea ice coverage.

Orvik and Skagseth (2003) analysed mooring data from the Svinoy section at around 64°N, and found correlations with the zonal mean wind stress curl at 55°N—close to the centre of our wind stress anomaly—with a time lag of 15 months. They attribute this time lag to forced baroclinic Rossby waves interacting with bathymetry causing a barotropic adjustment with fast topographic waves. Propagation of this speed is also found in singular events in our data (e.g. Fig. 12 around year 4435). As has been demonstrated by Döscher et al. (1994), these waves are poorly represented in a coarse resolution rigid-lid model on the Arakawa B-grid. Thus, adjustment in our model is mainly achieved by means of slower advective/diffusive processes.

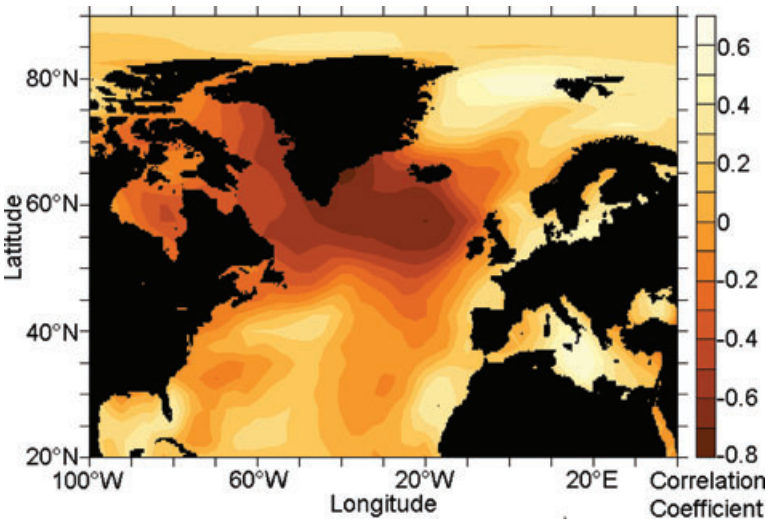


*Fig. 13.* Correlation between surface air temperature at (75°N; 5°W) and 10 yr leading surface air temperatures in the North Atlantic, calculated from NCEP reanalysis data from 1948 to 2005. Highest negative correlation coefficients occur over Greenland and in the south of Iceland.

Hátún et al. (2005) investigated the influence of the subpolar gyre on the thermohaline circulation in a high resolution ocean circulation model. They found an instantaneous weak salt export into the Rockall Trough, Faroe Current and Irminger Current in case of a strong subpolar gyre. While our studies confirm these findings in the Irminger Sea, we generally find the reaction in the Rockall Trough and Faroe Current at a delayed time, which is sometimes also observable in their Fig. 2B (e.g. in 1975). The propagation of this anomaly in our study is obvious in Fig. 12.

Our findings suggest that measurements of the subpolar gyre or the surrounding surface air temperature, respectively, could act as a predictor for sea ice coverage and Arctic temperatures. Fig. 13 shows an attempt to prove in how far one can trust these predictabilities by having a look at the NCEP reanalysis data (Kalnay et al., 1996). Here we took the surface air temperature in the Greenland Sea (75°N, 5°W) and searched for lagged correlations with the surface air temperature in other regions. Highest negative correlations actually occurred over Greenland and in the region south of Iceland where we applied the wind stress forcing in the model, though with a time shift of 10 instead of 9 yr. This slight difference can be explained by the different time spans considered. While the NCEP data involves just 58 yr, each of our model runs consists of 1000 yr. However, this kind of test was mainly made to see whether our tendency is mimicked in real world data.

The results should still be handled with care and further studies be made because of different reasons. For example, we use a simple atmospheric model and do not take the realistic NAO but just an NAO-like forcing, as mentioned above. On the other hand, due to the coarse resolution the topography in the Nordic Seas more or less consists of just one big basin, e.g. there is no Faroe Bank Channel. Further studies with the more advanced atmospheric compartment of the PlanetSimulator (Fraedrich et al., 2005) replacing the energy-moisture balance model of the pristine UVic ESCM will include more realistic forcing patterns and atmospheric feedbacks.

## 6. Acknowledgments

This work was funded by the German Science Foundation within the framework of the Collaborative Research Centre 512 'Cyclones and the North Atlantic Climate System'.

## References

Born, A., Levermann, A. and Mignot, J. 2009. Sensitivity of the Atlantic ocean circulation to a hydraulic overflow parameterisation in a coarse resolution model: response of the subpolar gyre. *Ocean Modell.* **27**, 130–142.

Cavazos, T. 2000. Using self-organizing maps to investigate extreme climate events: an application to wintertime precipitation in the Balkans. *J. Clim.* **13**, 1718–1732.

Cooper, L. H. N. 1955. Deep water movements in the North Atlantic as a link between climatic changes around Iceland and biological productivity of the English Channel and Celtic Sea. *J. Mar. Res.* **14**, 347–362.

Döscher, R., Böning, C. W. and Herrmann, P. 1994. Response of circulation and heat transport in the North Atlantic to changes in thermohaline forcing in northern latitudes: a model study. *J. Phys. Oceanogr.* **24**, 2306–2320.

Döscher, R. and Beckmann, A. 2000. Effects of a bottom boundary layer parameterization in a coarse-resolution model of the North Atlantic Ocean. *J. Atmos. Oceanic Technol.* **17**, 698–707.

Fraedrich, K. and Blender, R. 2003. Scaling of atmosphere and ocean temperature correlations in observations and climate models. *Phys. Rev. Lett.* **90**, 108501.

Fraedrich, K., Jansen, H., Kirk, E., Luksch, U. and Lunkeit, F. 2005. The planet simulator: towards a user friendly model. *Meteorol. Z.* **14**, 299–304.

Girton, J. B., Sanford, T. B. and Käse, R. H. 2001. Synoptic sections of the Denmark strait overflow. *Geophys. Res. Lett.* **28**(8), 1619–1622.

Greatbatch, R. J. 2000. The North Atlantic Oscillation. *Stoch. Environ. Res. Risk Assess.* **14**, 213–241.

Häkkinen, S. and Rhines, P. B. 2004. Decline of subpolar North Atlantic circulation during the 1990s. *Science* **304**, 555–559.

Hátún, H., Sandø, A. B., Drange, H., Hansen, B. and Valdimarsson, H. 2005. Influence of the Atlantic subpolar gyre on the thermohaline circulation. *Science* **309**, 1841–1844.

Hilmer, M. and Jung, T. 2000. Evidence for a recent change in the link between the North Atlantic Oscillation and Arctic sea ice export. *Geophys. Res. Lett.* **27**, 989–992.

Hooge, F. N. 1976. 1/f noise. *Physica B* **83**, 14–23.

Hurrell, J. W., 1996. Influence of variations in extratropical wintertime teleconnections on Northern Hemisphere temperature. *Geophys. Res. Lett.* **23**, 665–668.

Kalnay, E., Kanamitsu, M., Kistler, R., Collins, W., Deaven, D. and co-authors. 1996. The NCEP/NCAR 40-Year Reanalysis Project. *Bull. Am. Meteorol. Soc.* **77**(3), 437–472.

Käse, R. H. and Oschlies, A. 2000. Flow through Denmark Strait. *J. Geophys. Res.* **105**(28), 527–528, 546.

Kaulakys, B. and Meškauskas, T. 1999. On the generation and origin of 1/f noise. *Nonlinear Analysis: Modelling and Control, Vilnius, IMI* **4**, 87–96.

Köberle, C. and Gerdes, R. 2003. Mechanisms determining the variability of Arctic Sea Ice conditions and export. *J. Climate* **16**, 2843–2859.

Kösters, F. 2004. Denmark strait overflow: comparing model results and hydraulic transport estimates. *J. Geophys. Res.* **109**, C10011.

Kösters, F., Käse, R. H., Schmittner, A. and Herrmann, P. 2005. The effect of Denmark Strait overflow on the Atlantic meridional overturning circulation. *Geophys. Res. Lett.* **32**, L04602.

Latif, M., Böning, C., Willebrand, J., Biastoch, A., Dengg, J., and co-authors. 2006. Is the thermohaline circulation changing? *J. Clim.* **19**, 4631–4637.

Levitus, S., 1982. Climatological atlas of the world ocean. NOAA Prof. Pap. **13**, 173 pp. U.S. Government Printing Office, Washington DC.

Meehl, G. A., Tebaldi, C. and Nychka, D. 2004. Changes in frost days in simulations of twentyfirst century climate. *Clim. Dyn.* **23**(5), 495–511.

Montoya, M., Griesel, A., Levermann, A., Mignot, J., Hofmann, M. and co-authors. 2005. The Earth System Model of Intermediate Complexity CLIMBER-3$\alpha$. Part I: description and performance for present-day conditions. *Clim. Dyn.* **25**, 237–263.

Orvik, K. A. and Skagseth, ø. 2003. The impact of the wind stress curl in the North Atlantic on the Atlantic inflow to the Norwegian Sea toward the Arctic. *Geophys. Res. Lett.* **30**(17), 1884.

Pacanowski, R. 1995. MOM 2 documentation: User's guide and reference manual. *GFDL Ocean Group Tech. Rep.* **3**, 232 pp.

Quadfasel, D. and Käse, R. 2007. Present-day manifestation of the Nordic Seas Overflows. In: *Ocean Circulation: Mechanisms and Impacts*, (eds A. Schmittner, J. C. H. Chiang and S. R. Hemmings), Geophys. Monogr. Ser. **173**, AGU, Washington DC, 75–89.

Reid, P. C., Borges, M. F. and Svendsen, E. 2001. A regime shift in the North Sea circa 1988 linked to changes in the North Sea horse Mackerel fishery. *Fisher. Res.* **50**, 163–171.

Roemmich, D. and Wunsch, C. 1985. Two transatlantic sections: meridional circulation and heat flux in the subtropical North Atlantic Ocean. *Deep Sea Res.* **32**(6), 619–664.

Ross, C. K. 1984. Temperature-salinity characteristics of the 'overflow' water in Denmark Strait during 'OVERFLOW 73'. *Rapp. P.-v. Reun. Cons. Int. Explor. Mer.* **185**, 111–119.

Saenko, O. A., Weaver, A. J. and Schmittner, A. 2003. Atlantic deep circulation controlled by freshening in the Southern Ocean. *Geophys. Res. Lett.* **30**, 1734.

Saunders, P. M., Cunningham, S. A., de Cuevas, B. A. and Coward, A. C. 2008. Comments on "Decadal Changes in the North Atlantic and Pacific Meridional Overturning Circulation and Heat Flux". *J. Phys. Oceanogr.* **38**, 2104–2107.

Spence, J. P., Eby, M. and Weaver, A. J. 2008. The Sensitivity of the Atlantic meridional overturning circulation to freshwater forcing at eddy-permitting resolutions. *J. Climate* **21**, 2679–2710.

Talley, L. D., Reid, J. L. and Robbins, P. E. 2003. Data-based meridional overturning streamfunctions for the global ocean. *J. Climate* **16**, 3213–3226.

Weaver, A. J., Eby, M., Wiebe, E. C., Bitz, C. M., Duffy, P. B. and co-authors. 2001. The UVic earth system climate model: model description, climatology, and applications to past, present and future climates. *Atmos. Ocean* **39**, 361–428.

Wiebe, E. C. and Weaver, A. J. 1999. On the sensitivity of global warming experiments to the parametrisation of sub-grid scale ocean mixing. *Clim. Dyn.* **15**, 875–893.

Whitehead, J. A. 1998. Topographic control of oceanic flows in deep passages and straits. *Rev. Geophys.* **36**, 423–440.

Yano, J.-I., Fraedrich, K. and Blender, R. 2000. Tropical convective variability as 1/f noise. *J. Climate* **14**, 3608–3616.